THE ASTROPHYSICAL JOURNAL, 287:801–813, 1984 December 15

NEAR-INFRARED SPECKLE INTERFEROMETRY OF EVOLVED STARS AND BIPOLAR NEBULAE

H. M. DYCK,[1, 2, 3] B. ZUCKERMAN,[3, 4] CH. LEINERT,[1, 3] AND S. BECKWITH[3, 5]

Received 1984 March 20; accepted 1984 June 5

ABSTRACT

We present near-infrared (1.65–4.8 μm) spatial visibility data for 16 late-type stars and bipolar nebulae. The majority of the sample are partially resolved and have linear radii averaging about 10^{15} cm at 3.8 μm. The measured angular diameters at 3.8 μm are in good agreement with predictions of dust-shell boundaries in the models of Rowan-Robinson and Harris. We interpret these observations as general confirmation of the assumption that there is a dust-free zone which extends out to a few stellar radii in the circumstellar envelope. Stars with the most extensive wavelength coverage clearly show a systematic increase of angular size proportional to a power of the wavelength. The observed size increase is apparently steeper for oxygen-rich stars than for carbon stars. From the limited data available, we have found that the infrared angular diameters lie between those observed for the SiO and H_2O masing regions but are a factor ~ 50 smaller than those observed for OH. Stars with the highest mass loss rates have the largest observable angular diameters. Our observations in two orthogonal directions show deviations from circular symmetry only for the most spatially resolved objects in the infrared. For the remaining objects the apparent symmetry may be the result of inadequate spatial resolution.

Subject headings: infrared: sources — interferometry — nebulae: general — stars: diameters — stars: late-type — stars: mass loss

I. INTRODUCTION

At about the time of their discovery, the reddest objects in the CIT 2 μm sky survey (Neugebauer and Leighton 1969) were recognized as late-type stars surrounded by extensive dust envelopes (McCammon, Münch, and Neugebauer 1967). Neugebauer, Martz, and Leighton (1965) pointed out that NML Cyg, for example, if interpreted as a blackbody, must have an infrared angular diameter of 0".08. Shortly thereafter dust envelopes surrounding normal, cool giants and supergiants were discovered to be a general phenomenon (Gillett, Merrill, and Stein 1971). It was postulated (Gehrz and Woolf 1971; Hyland *et al.* 1972) that the underlying stars themselves created the dust as an integral part of the mass loss process, already (Deutsch 1960) thought to be ubiquitous among late-type stars. Thus commenced arguments, not yet settled, about whether the dust was the parent or the child of mass loss.

Recent radio observations have demonstrated that the total sizes of the envelopes are very extended indeed. Projected angular diameters range from a few arcsec, delineated by OH (Bowers, Johnston, and Spencer 1983), up to a few arcmin in CO (Knapp *et al.* 1982). Mass loss rates of order $10^{-4}\ M_\odot\ \mathrm{yr}^{-1}$ have been estimated for the most extreme examples.

Because of their relevance to interstellar chemistry and probable relationship, in some cases, to planetary nebulae, there has been considerable effort expended to understand the physical structure of the circumstellar envelopes (see, e.g., Rowan-Robinson and Harris 1983*a*, *b*; Kwan and Linke 1982). However, the basic observational data which define this structure close to the star are lacking. For example, it is not yet possible to say (1) where the dust is formed or (2) whether the density departs significantly from an inverse-square of the distance law, which one would expect from the simplest physical arguments. Both of these data are important if one is to understand the velocity structure and the coupling between grains and gas (Tielens 1983). Nor is it possible to say with certainty whether, or on what spatial scale, departures from spherical symmetry are important.

The development of infrared speckle interferometry has made available diffraction-limited information on large telescopes (Sibille, Chelli, and Léna 1979): At 2.2 μm with a 4 m telescope one can expect to resolve structure at about the 0".1 scale. Thus, for stars which are similar in photometric characteristics to NML Cyg one may expect to resolve the shells easily in the infrared. For the nearest of these stars this spatial resolution corresponds to a linear resolution of a few stellar photospheric radii. Using a speckle interferometry system, we have begun a study of the spatial brightness distribution at various wavelengths in the infrared, for a number of late-type stars. The purpose of this paper is to report the first results of the program. The observational sample consists primarily of OH/IR stars and carbon stars with millimeter-wave CO emission. We have included, for comparison, a number of additional objects which optically appear as bipolar structures on the sky. We discuss the results in terms of currently available circumstellar envelope models and in relationship to the radio observations. The list of observed objects is given in Table 1 along with estimated distances and mass loss rates and measured envelope expansion velocities taken from the literature.

II. OBSERVATIONS AND DATA REDUCTION

The data were obtained at Mauna Kea using speckle interferometry systems similar to the one described by Dyck and Howell (1982). Normal InSb photometers with broad-band *H*

[1] Max-Planck-Institut für Astronomie, Heidelberg.
[2] On leave from Institute for Astronomy, University of Hawaii.
[3] Visiting Astronomer at the Infrared Telescope Facility, which is operated by the University of Hawaii under contract with the National Aeronautics and Space Administration, and at the United Kingdom Infrared Telescope.
[4] Department of Astronomy, University of California, Los Angeles.
[5] Department of Astronomy, Cornell University.

TABLE 1

THE PROGRAM OBJECTS

Star	α(1950)	δ(1950)	Type	D (pc)	V_0 (km s^{-1})	$\dot{M}(M_\odot$ yr$^{-1})$	Ref.
CIT 5	03^{h}22^{m}58^s.8	+47°21′19″	C	680	18	2.2×10^{-5}	
NML Tau	03 50 43.7	+11 15 30	M8–M11	270	28	4.2×10^{-6}	
AFGL 618	04 39 33.8	+36 01 15	C	1700	18	2.7×10^{-4}	
AFGL 915	06 17 37.0	−10 36 52	B9–A0 III	330	...	...	1
VY CMA	07 20 54.8	−25 40 12	M5 I	1500	37	2.3×10^{-4}	2
OH 0739−14	07 39 58.9	−14 35 45	M6	2000	23	3.0×10^{-4}	
IRC +10216	09 45 14.8	+13 30 40	C9,5	290	17	1.5×10^{-4}	
CIT 6	10 13 11.0	+30 49 17	C4,3	190	17	3.2×10^{-6}	
M2-9	17 02 52.5	−10 04 32	O9–B1	1000	21	...	3
VX Sgr	18 05 03.0	−22 13 55	M4–M8 I	1500	20	2.4×10^{-5}	4
OH 26.5+0.6	18 34 52.5	−05 26 37	M	1100	14	2.6×10^{-5}	5
IRC +10420	19 24 27.0	+11 15 03	F8 I	3400	33	2.0×10^{-4}	2
M1-92	19 34 18.4	+29 26 05	B0.5 V	4500	30	...	6
χ Cyg	19 48 38.5	+32 47 12	S6,2–S10,4	97	8	1.8×10^{-7}	
V Cyg	20 39 41.3	+47 57 45	C7,4	610	14	2.5×10^{-5}	
NML Cyg	20 44 33.9	+39 55 57	M6	1800	28	1.6×10^{-4}	2

NOTE.—Unless otherwise noted, the distance (D), terminal envelope velocity (V_0), and mass loss rate ($\dot{M}$) were taken from the tabulations by Knapp *et al.* 1982 and Spergel, Giuliani, and Knapp 1983.

REFERENCES.—(1) Cohen *et al.* 1975. (2) Bowers, Johnston, and Spencer 1983. (3) Eiroa, Hefele, and Qian Zhong-yu 1983. Carsenty 1983. (4) V_0 taken from Baud and Habing 1983; $\dot{M}$ calculated from eq. (3) of Bowers, Johnston and Spencer 1983 using the observed angular OH radius (Baud 1981) and an adopted distance of 1500 pc. (5) Baud and Habing 1983. (6) Herbig 1975.

($\lambda_0 = 1.65$ μm, $\Delta\lambda = 0.3$ μm), K ($\lambda_0 = 2.2$ μm, $\Delta\lambda = 0.4$ μm), L' ($\lambda_0 = 3.8$ μm, $\Delta\lambda = 0.6$ μm), and M ($\lambda_0 = 4.8$ μm, $\Delta\lambda = 0.5$ μm) filters were used with a long, narrow slit placed in the focal plane just in front of the detector field optics. Slit widths of 0.077 and 0.154 mm were available, with the choice depending upon wavelength, object brightness, and seeing conditions. These two widths correspond approximately to the telescope diffraction limit, λ/D, for an f/35 beam at K and M, respectively, where D is the diameter of the telescope primary mirror. Three telescopes were used: All observations made in the north-south direction were obtained at the UH 2.2 m telescope. With one exception, all observations made in the east-west direction were obtained at the 3.8 m UKIRT. The one exception is the set of east-west observations of OH 0739−14; these data were obtained at the NASA 3 m telescope.

At each telescope, the image of a source to be measured is scanned repeatedly 100–128 times across the slit by driving the telescope secondary under computer control. The scan speed was adjusted to be fast enough to "freeze" the seeing pattern. Data are synchronously recorded with 128 sample points taken per scan line. The scan line lengths are typically 10″, but in this experiment they ranged from 5″ to 15″ depending upon source size and other factors. The data are fast Fourier transformed line-by-line, and the average source power spectrum, P_s, as a function of spatial frequency, f, is computed. Such an average power spectrum is the product of the power spectrum of the spatial brightness distribution of the source and the time-average of the square of the modulation transfer function ($\langle \mathrm{MTF}^2 \rangle$) of the atmosphere-telescope combination (see, e.g., Sibille, Chelli, and Léna 1979). By observing a nearby calibration star (which has an angular diameter $\ll \lambda/D$) one obtains its spatial power spectrum, P_c, which is simply the function $\langle \mathrm{MTF}^2 \rangle$ alone. When either object is faint, one must also observe a nearby region of the sky to measure the noise power, P_n, which is then subtracted from the object power. Division of P_s by P_c after correction for noise power, if necessary, yields the power spectrum of the spatial brightness distribution of the source alone, provided the seeing has remained constant. In the remainder of the paper we will discuss source visibilities defined by the square root of this power ratio.

When the errors are negligible, the source visibility, $V(f)$, is the modulus of the spatial frequency spectrum of the source brightness distribution. Serious errors can arise from two principal sources: variation in seeing and inaccuracies in the motion of the telescope secondary. Seeing artifacts in the derived visibilities sometimes provide a persistent source of systematic error (Mariotti *et al.* 1983). It has been noted by these authors and by Sibille, Chelli, and Léna (1979) that fluctuations of seeing can produce visibilities which may be interpreted as extended halos around stars. One must, therefore, be extremely careful to alternate frequently between source and calibrator and to observe for a sufficiently long time that seeing effects are averaged out. The convergence of the power spectra under fluctuating seeing conditions was carefully monitored in real time at the telescope. Later data processing yielded additional, quantitative information about the effect of seeing variations: In this technique one divides calibrator by calibrator and source by source, taken in the same sequence as the computation of the source visibility, and averages the result. This average would be unity at all spatial frequencies, in the absence of seeing variations. Any departure from unity gives a measure of the absolute level and the form of the residual systematic errors. Our experience has been that this average can deviate by ±10% from unity for bright, seeing-limited objects (i.e., when speckle noise is the dominant noise source). Thus any visibility which smoothly drops below 90% at the highest spatial frequency can be considered to be at least partially resolved. This limit has been found to be approximately $\frac{1}{4}$ of λ/D in practice. Apart from the systematic errors, variable seeing is also the principal source of random errors for bright objects where speckle noise dominates. From the scatter in fits of Gaussian visibilities to partially resolved sources, we estimate that the standard error of a single seeing-limited observation lasting from 3 to 5 minutes (i.e., several sets of 100–128 scans) is ±0.″015 in the measured full width at half-maximum (FWHM).

Inaccuracies in the motion of the scanning secondary mirror occur either as noise (i.e., jitter) in the scanning motion or as variations in the length/velocity of a scan from one scan to the next. The first of these effects adds power at higher spatial frequencies to the source spatial power spectrum (Leinert and Dyck 1983) and is not detectable when one measures noise on the sky. The effect can be very serious but cannot easily be removed because it is dependent upon the source brightness geometry. When a telescope secondary mirror suffers from this problem, the source visibilities will asymptotically approach a constant level $0 \leq V(f_j) \leq 1$ for $f \geq f_j$, where f_j is some critical frequency imposed by the jitter. For $f < f_j$ the telescope produces accurate visibilities. One can detect the effect in visibilities of known geometries such as double stars and extended sources and, hence, determine f_j. Data taken at the IRTF were so affected; consequently, the data for OH 0739 − 14 were truncated beyond $f_j = 1$ cycle arcsec^{-1}. The data taken in 1982 June on the UKIRT, with a hydraulically driven secondary, also show this problem and were truncated at $f_j = 1.9$ cycles arcsec^{-1}. Data taken in 1983 May on the UKIRT, after a new electrically driven secondary was installed, are free of this noise problem. All data obtained with the UH telescope are free of the problem.

The second source of scanning-mirror error has the effect of averaging over the source visibility. We conclude from observations of visual double stars that the effect of the velocity variations is completely negligible.

Apart from the limitations described above, the highest spatial frequencies available were determined by either the telescope diffraction limit or the transfer function for the slit. We have truncated the data above frequencies at which the computed telescope MTF (without seeing effects) or the slit function, approximated by sinc (πwf), where w is the slit width in arcsec, drops to 0.1, whichever frequency is lower. In the former case this frequency corresponds approximately to the Rayleigh criterion, $f_R = D(1.22\lambda)$.

During the scan process we compute the integral of each scan line, after removing the baseline. This integral is proportional to the flux received so that, in principle, we can compute the object brightness in standard units. In practice this is limited by inadequate standards or by partly cloudy weather, when it is still possible to do speckle interferometry. We have listed object brightnesses in magnitudes in Table 2,

TABLE 2

MAGNITUDES DERIVED FROM THE SCANS

Star	UT Dates	K	L'	M
CIT 5	1981 Oct 8	...	...	−1.1
VY CMa	1981 Oct 11	..	−2.9	...
IRC +10216	1983 May 14–24	0.8	...	...
CIT 6	1983 May 13–26	1.2	−2.1	−3.0
VX Sgr	1983 May 17	...	−1.7	...
OH 26.5+0.6	1982 Jun 28–30	...	0.8	(−0.7)
	1983 May 13	...	1.8	...
IRC +10420	1983 May 13–24	3.4	0.8	−0.2
χ Cyg	1983 May 25–30	...	...	(−3.0)
NML Cyg	1981 Oct 10	...	−2.0	...
	1982 Jun 26	...	...	(−2.8)
AFGL 915	1980 Nov 28	...	...	0.1
	1982 Nov 25–26[a]	3.4	1.1	(0.3)
AFGL 618	1982 Nov 25	...	4.9	...
M2-9	1983 May 24–30	...	3.6	...
M1-92	1983 May 14–25	...	3.4	...

[a] $H = 5.1$.

obtained when conditions permitted. They are generally accurate to ±10% except when enclosed by parentheses, which indicate ±20% accuracy. In all cases the observed signal-to-noise ratio is 50–100, and the errors arise from calibration uncertainties.

The observations are plotted in Figures 1–14 as visibility versus spatial frequency[6] in cycles arcsec^{-1}. In most cases these visibility functions are averages of several observations, lasting from 2 to 6 minutes, each of which is treated independently. Often the data were obtained on several nights and, in a few cases, during different observing periods. The error bars are ±1 standard error of the mean, computed from the observational scatter, and are shown only if they exceed ±0.03 in visibility. When only a single observation existed, we computed the errors from the scatter in the subsets of 100–128 scans each. We have also fitted simple models to the visibility data. With three exceptions the model visibility functions are

$$V(f) = V_0 \exp(-3.57 f^2 \theta^2), \quad (1)$$

where V_0 is the visibility at $f = 0$, and θ is the characteristic full width at half-maximum (FWHM) of the brightness distribution in object space. The logarithmic form of this equation has been fitted to the data by least squares to determine V_0 and θ. The fits were done first to each independent set of data in order to estimate the scatter in the two parameters. The models shown, however, correspond to fits to the average visibility functions. The results of the fits to these averages are listed in Table 3 as θ and V_0, where the quoted errors are ±1 standard error of the mean of the independent data sets, when more than one set existed. When only one set of data was available, we have quoted the mean error for a seeing-limited observation, mentioned above—namely, ±0.″015 in θ and ±0.03 in V_0.

We have chosen Gaussian visibility functions because they are easy to compute, not because they are physically realistic. For the partially resolved sources described in this paper, such an assumption is unimportant. This is true because it is easy to overlay visibility functions for completely different spatial brightness distributions in the low-frequency range simply by adjusting the size parameter. This has previously been noted by Reid, Moran, and Johnston (1981) and by Allen, Barton, and Wallace (1981). Thus, for slightly resolved sources, one can convert mathematically simple models to physically realistic ones with no loss of information by applying the correct scaling factor. Conversely, because of this non-uniqueness in the models at low frequencies, choosing a more complex mathematical form is not rational unless one has a good physical basis for doing so. So, for example, it would be appropriate to compare our observations with the predicted visibilities from the extensive models computed by Rowan-Robinson and Harris (1982, 1983*a*, *b*), Lefèvre, Bergeat, and Daniel (1982), and Lefèvre, Daniel, and Bergeat (1983) to match the observed fluxes from cool stars. Such a procedure has already been followed by Tsuji (1979), who used his dust-shell models to match interferometric data for α Ori.

There are three objects for which multiple-component models are required (or, at least, the simple one-component Gaussian models clearly do not fit): These are IRC +10216, OH 0739 − 14, and AFGL 915 (the Red Rectangle). Interpretation of the visibility data for these three objects is contained in the following section.

[6] The frequency scale was calibrated through observations of visual double stars of known separation. From the scatter in these measurements we estimate the error in the frequency scale to be ±2.5%.

TABLE 3

SUMMARY OF GAUSSIAN-MODEL FITS TO THE DATA

OBJECT	λ (μm)	NORTH-SOUTH		EAST-WEST		T (N)[a]
		$\theta \pm \epsilon$(″)	$V_0 \pm \epsilon$	$\theta \pm \epsilon$(″)	$V_0 \pm \epsilon$	
CIT 5	3.8	0.008 ± 0.015	0.93 ± 0.03	...	...	8.0 (10)
	4.8	0.071 ± 0.015	0.94 ± 0.03	...	...	6.4 (8)
NML Tau	3.8	0.054 ± 0.015	1.03 ± 0.03	...	...	4.8 (6)
AFGL 618	3.8	0.13 ± 0.04	0.96 ± 0.04	...	...	9.6 (12)
AFGL 915[b]	1.6	0.0	0.39 ± 0.03	...	...	9.6 (12)
		0.86 ± 0.08	0.63 ± 0.02	...	...	
	2.2	0.078 ± 0.016	0.47 ± 0.01	...	...	15.2 (19)
		0.78 ± 0.04	0.53 ± 0.02	...	...	
	3.8	0.129 ± 0.004	0.59 ± 0.03	...	...	8.8 (11)
		0.94 ± 0.11	0.42 ± 0.02	...	...	
	4.8	0.163 ± 0.004	0.67 ± 0.01	...	...	8.8 (11)
		0.92 ± 0.09	0.33 ± 0.02	...	...	
VY CMa	3.8	0.118 ± 0.015	0.88 ± 0.03	...	...	5.6 (7)
	4.8	0.137 ± 0.021	0.94 ± 0.01	...	...	6.4 (8)
OH 0739−14[b]	3.8	0.58 ± 0.08	0.34 ± 0.01	0.39 ± 0.14	0.37 ± 0.01	11.2 (16)
		3.5 ± 1.2	0.66 ± 0.12	2.3 ± 0.2	0.63 ± 0.04	
IRC +10216[b]	2.2	0.0	0.22 ± 0.04	0.0	0.22 ± 0.04	17.5 (25)
		0.40 ± 0.05	0.54 ± 0.04	0.22 ± 0.02	0.49 ± 0.05	
		1.1 ± 0.2	0.27 ± 0.05	1.1 ± 0.2	0.27 ± 0.05	
CIT 6	2.2	0.063 ± 0.010	1.00 ± 0.01	0.077 ± 0.005	1.02 ± 0.03	20.1 (27)
	3.8	0.102 ± 0.015	0.99 ± 0.03	...	...	5.6 (7)
	4.8	0.144 ± 0.015	0.94 ± 0.03	...	...	3.2 (4)
M2-9	3.8	0.113 ± 0.025	0.97 ± 0.03	0.062 ± 0.024	0.91 ± 0.01	21.2 (30)
VX Sgr	2.2	0.051 ± 0.007	0.97 ± 0.01	...	...	10.4 (13)
	3.8	0.095 ± 0.006	0.95 ± 0.02	...	...	6.4 (8)
OH 26.5+0.6	3.8	0.074 ± 0.019	0.99 ± 0.02	0.099 ± 0.015	1.01 ± 0.03	21.7 (28)
	4.8	0.159 ± 0.015	0.96 ± 0.03	0.107 ± 0.015	0.95 ± 0.03	10.1 (14)
IRC +10420	2.2	0.074 ± 0.005	0.83 ± 0.03	0.072 ± 0.002	0.83 ± 0.02	16.2 (20)
	3.8	0.155 ± 0.024	0.93 ± 0.02	0.118 ± 0.013	0.87 ± 0.01	23.9 (33)
	4.8	0.190 ± 0.007	0.92 ± 0.02	0.154 ± 0.001	0.86 ± 0.01	14.2 (19)
M1-92	3.8	0.071 ± 0.023	0.92 ± 0.03	0.053 ± 0.027	0.97 ± 0.06	13.8 (19)
	4.8	...	...	≤0.057	0.98 ± 0.04	4.0 (6)
χ Cyg	2.2	...	...	0.031 ± 0.015	1.01 ± 0.03	2.0 (3)
	4.8	0.107 ± 0.015	1.02 ± 0.03	0.075 ± 0.007	0.94 ± 0.03	9.2 (13)
V Cyg	3.8	≤0.045	1.00 ± 0.03	...	...	3.2 (4)
NML Cyg	2.2	0.079 ± 0.008	0.85 ± 0.03	...	...	13.6 (17)
	3.8	0.135 ± 0.025	0.93 ± 0.04	...	...	4.8 (6)
	4.8	0.188 ± 0.015	0.94 ± 0.03	0.151 ± 0.006	0.96 ± 0.01	10.8 (15)

[a] T = the time in minutes spent observing the source alone (without calibrator); N = the number of independent measures of the source.

[b] Errors in the models were not determined by the dispersion in fits to independent data sets. See text for details.

III. DISCUSSION

a) *The Evolved Giants and Supergiants*

i) *CIT 5*

This carbon star is unresolved at L' (3 σ upper limit $\theta \leq 0''.045$) but partially resolved at M in the north-south direction (Fig. 1). We have found no other size measurements reported in the literature. The brightness is variable (Merrill and Stein 1976). The measured brightness indicates that the star was relatively faint at the time of our observation.

ii) *NML Tauri*

Our single L' observation has not been plotted in a figure. A least squares fit to the data yields $\theta = 0''.054 \pm 0''.015$ and $V_0 = 1.03 \pm 0.03$. Howell Howell (1980) reported NML Tau to be partially resolved at 11.6 μm.

iii) *VY Canis Majoris*

We have resolved a shell at L' and M (Fig. 2); there is a suggestion that the size is slightly larger at M than at L'. We do not see any strong evidence for large-scale extended structure similar to that seen by Herbig (1972) in visual photographs. However, the least squares fit Gaussian at L' intersects the visibility axis at $V_0 = 0.88$, indicating that about 12% of the observed flux could arise from an extended halo with dimensions $\theta = 3''$. More careful observations will be needed to determine whether this structure is real or simply a seeing artifact.

Previous spatial interferometry measurements between 5.0 μm and 11.1 μm were reported by Low (1979); his 5.0 μm diameter of $\theta = 0''.16$ is consistent with our 4.8 μm datum in Table 3. In his thesis, Howell (1980) gives an upper limit of $0''.15$ at 2.2 μm and $\theta = 0''.75$ at 12 μm. Sutton *et al.* (1977) reported $\theta = 0''.48$ at 11.1 μm. Thus, it is clear that the apparent size increases systematically with increasing wavelength. McCarthy (1979) reported a noncircular projected shape at 10.2 μm with an axial ratio of 1.5.

iv) *IRC +10216*

Extensive spatial brightness distribution measurements of this star have been reported by Toombs *et al.* (1972), Sutton *et al.* (1979), Selby, Wade, and Sanchez Magro (1979), McCarthy, Howell, and Low (1980), and Mariotti *et al.* (1983). Our data

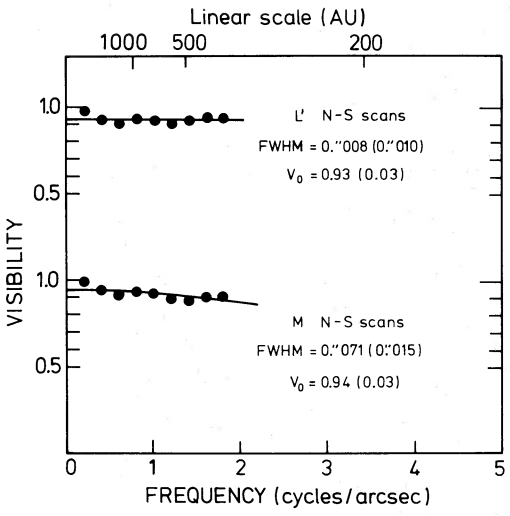

FIG. 1

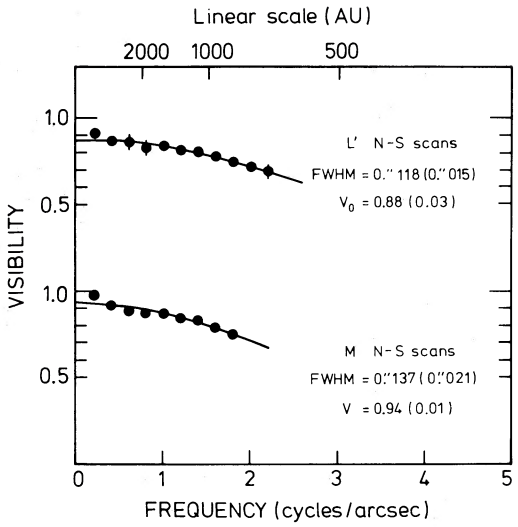

FIG. 2

FIG. 1.—Visibility functions for CIT 5. Single-component Gaussian models, with the indicated FWHM, have been fitted to the data but not forced to unity at spatial frequency zero. The parameter V_0 is the value of the visibility model at zero frequency. The numbers in parentheses are $\pm$ 1standard error of the mean.

FIG. 2.—The same as in Fig. 1 except for VY CMa

are presented as a comparison to the work of these others. They indicate also that visibilities can be complex and demonstrate the possible problems one may encounter when interpreting partially resolved sources with simple models.

The visibilities illustrate a fact that has already been emphasized (McCarthy, Howell, and Low 1980; Howell 1980): The brightness distribution is markedly different in the two orthogonal directions. The sense of the difference is that the brightness is more extended north-south than east-west, although the interpretation is not simple. When one overlays the two visibility curves one finds good agreement in the frequency range $0 \leq f$ (cycles arcsec^{-1}) ≤ 0.62. That means that the 2.2 μm brightness is reasonably circularly symmetric on spatial scales $\theta \geq 1\farcs6$. Approximately one-fourth of the total 2.2 μm flux comes from this extended region, which we believe may be scattered light in the outer envelope. In the frequency range $0.62 \leq f$ (cycles arcsec^{-1}) ≤ 3.2 the two curves are divergent. The north-south visibility drops to a constant level $V = 0.22$ at $f = 2.2$ cycles arcsec^{-1}. The east-west visibility falls more gradually to a constant level $V = 0.30$ at $f = 3.2$ cycles arcsec^{-1}. Thus on a spatial scale $0\farcs3 \leq \theta \leq 1\farcs6$ the brightness is more extended north-south than east-west by about a factor of 2. Approximately one-half of the 2.2 μm flux comes from this region of intermediate spatial scale. At the highest spatial frequencies the visibilities in both directions are approximately constant, indicating the presence of a compact component (which we presume to be the underlying star) contributing about one-fourth of the flux. Inspection of the north-south visibility shows that this compact component is completely unresolved in our measurements. In Figure 3 we have shown the visibility for a three-component model which reproduces the features discussed above. The model parameters are summarized in Table 3. For this case the errors are determined from the range of fits permitted by the errors on the individual frequency points. We also note that this model is quite similar, qualitatively, to the one developed by Toombs *et al.* (1972) to account for their lunar occultation data. At 2.2 μm they propose an outer halo contributing 10%–20% of the flux with a Gaussian $\theta = 1\farcs2$ and a smaller region ($\theta = 0\farcs22$) contributing most of the remainder. They report that as much as 20% of the flux could come from an unresolved component. We emphasize that the three-component model used here need not be taken literally. Rather, the Fourier transform of the synthesized visibility gives one possible representation of the brightness distribution in object space.

It has already been reported (McCarthy, Howell, and Low 1980) that the apparent size of the envelope changes with time. This is obvious when our 2.2 μm data are compared with those reported by others. For example, our east-west visibility is nearly identical to that observed by Howell (1980), but our two sets of north-south data are significantly different. The 2.2 μm north-south visibility reported by Selby, Wade, and Sanchez

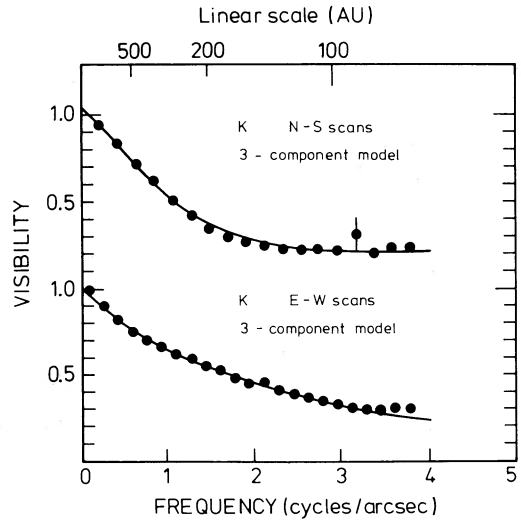

FIG. 3.—Visibility functions for IRC +10216. The solid lines represent a three-component model discussed in the text.

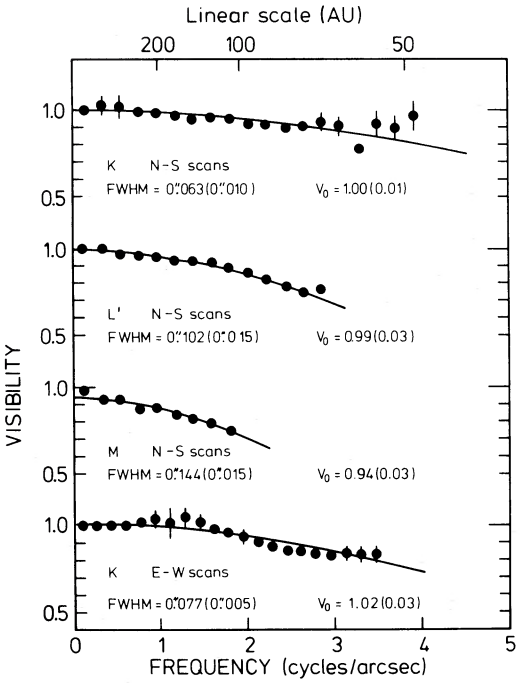

FIG. 4.—The same as in Fig. 1 except for CIT 6

Magro (1979) differs from both our data and Howell's data. It is possible that the variations are more pronounced in the north-south direction.

Finally, it is of interest to ask how IRC +10216 would appear if it were more distant. At 5 times its distance—D = 1450 pc, or somewhat greater than the average distance of all the sources in Table 1—the source would be only partially resolved. A least squares fit of a Gaussian to such a visibility yields an excellent fit, with $\theta = 0''.089$ north-south and $\theta = 0''.084$ east-west. At the present resolution, a distant IRC +10216 would be well represented by our simple model and would appear identical in the two orthogonal directions. Thus, one must be careful in drawing conclusions about the apparent symmetry in partially resolved sources.

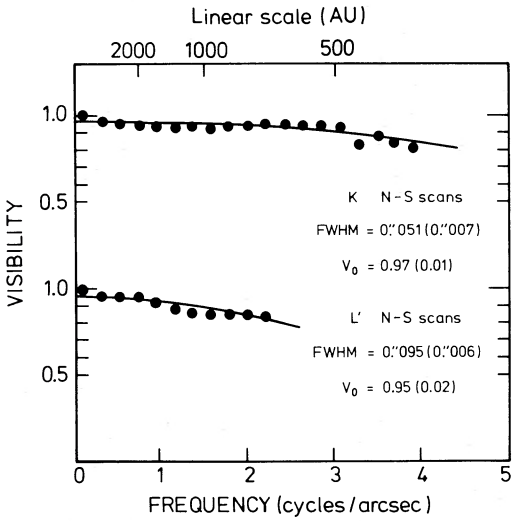

FIG. 5.—The same as in Fig. 1 except for VX Sgr

v) *CIT 6*

Our data are plotted in Figure 4. The north-south visibilities nicely illustrate the increase in the apparent angular size with increasing wavelength already noted for VY CMa. Comparison of the north-south and east-west data shows that the two θ agree to within the errors; we find $\theta_{NS}/\theta_{EW} = 0.82 \pm 0.13$. Thus, there is no obvious asymmetry at our spatial resolution. CIT 6 has also been observed by Low (1979) between 8.4 μm and 12.5 μm and by Mariotti *et al.* (1983), who only report an upper limit $\theta \leq 0''.14$ at 4.6 μm. Howell (1980) reported upper limits at 2.2 μm and 4.8 μm of 0".3 and 0".25, respectively.

vi) *VX Sagittarii*

Our north-south visibility data are shown in Figure 5; a shell is partially resolved at both wavelengths. The measured size at L' is larger than that at K. This star was previously reported to be unresolved by Low (1979).

vii) *OH 26.5+0.6*

We observed this star on three different occasions between 1981 October and 1983 May. There is some evidence in the L' data that the size is variable, although more precise observations will be needed to decide this point. With this precautionary statement we have, nevertheless, averaged all the data together and plotted them in Figure 6. The shell appears to be larger at M than at L'. At L' we detect no significant difference between the north-south and east-west sizes; we find $\theta_{NS}/\theta_{EW} = 0.75 \pm 0.22$. AT M the difference between the two directions is about twice the combined errors. The ratio is $\theta_{NS}/\theta_{EW} = 1.50 \pm 0.25$. Mariotti *et al.* (1983) have also reported 4.6 μm interferometry: At a position angle P.A. = 90° they obtained an upper limit $\theta \leq 0''.11$, about equal to our measured east-west value at M. At P.A. = 150°, roughly comparable to our north-south data, they found $\theta = 0''.12 \pm 0''.04$, consistent with our measurement. Perrier (1982) has found $\theta = 0''.088 \pm 0''.013$ at 4.6 μm.

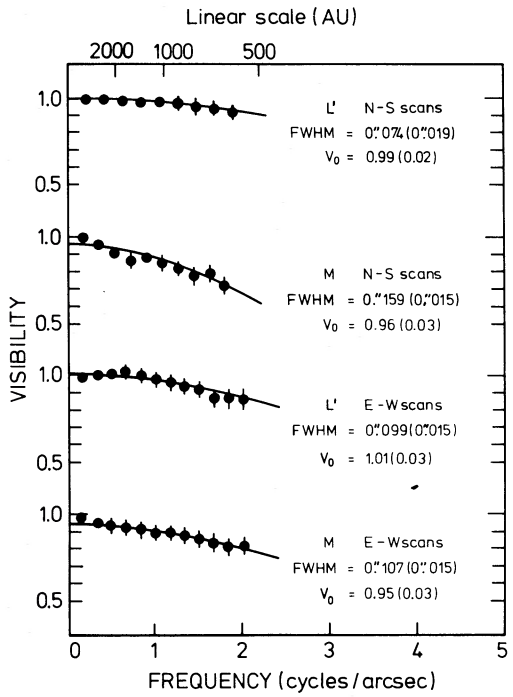

FIG. 6.—The same as in Fig. 1 except for OH 26.5+0.6

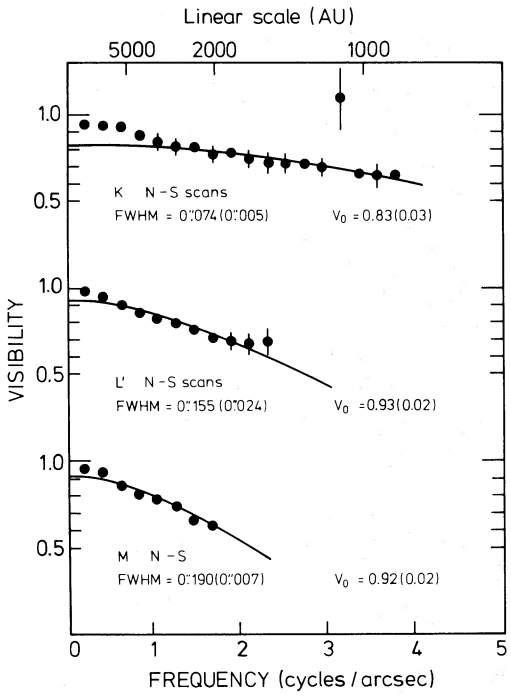

FIG. 7.—The same as in Fig. 1 except for IRC +10420

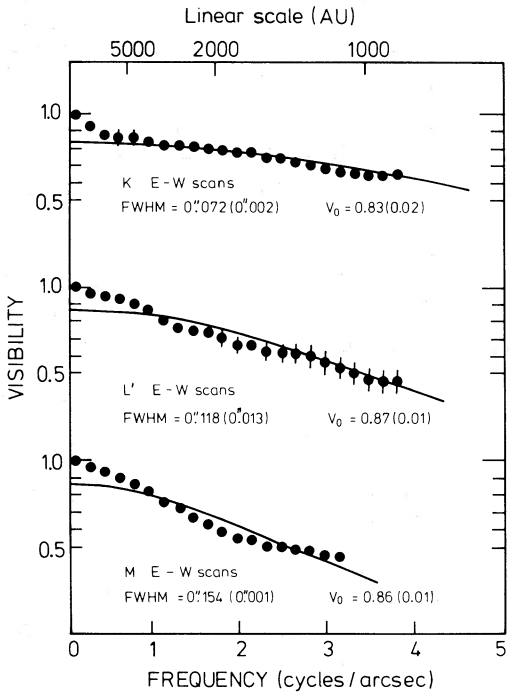

FIG. 8.—The same as in Fig. 1 except for IRC +10420

viii) *IRC +10420*

We have plotted our three-color north-south visibilities in Figure 7; the east-west data are shown in Figure 8. Although the separate Gaussian fits to the north-south and east-west data in the figures indicate differences at L' and M, this is mainly the result of differences in the highest spatial frequencies, which could not be reached by the 2.2 m telescope in the north-south direction. In fact, when one overlays the visibilities for the two orthogonal directions, one cannot visually detect any significant difference. By fitting visibilities over the same frequency range east-west and north-south, we obtain $\theta_{NS}/\theta_{EW} = 1.02 \pm 0.18$ at L' and $\theta_{NS}/\theta_{EW} = 0.91 \pm 0.03$ at M. Thus, at comparable spatial resolution in the two directions there is no strong evidence for asymmetry. Both directions show the systematic increase in apparent angular size with wavelength already reported for other stars. Previously, Low (1979) published measurements between 5.0 μm and 12.5 μm.

IRC +10420 apparently also has a large-scale halo surrounding the compact thermal shell. It is more obvious at K. We believe that this is real and not an artifact of seeing because the standard stars measured at the same time do not show any such effect. The halo size at K is of order $\theta = 1''.3$, and its contribution to the flux (about 17% at K) is less at longer wavelengths. This is consistent with the interpretation that the halo results from scattering.

ix) χ *Cygni*

Our data are plotted in Figure 9. A shell has been resolved at M in both the north-south and east-west directions. The difference in the model fits shown in the figure is again a result of differences in the highest spatial frequencies observed in the two directions. When models are fitted over equal frequency ranges, we obtain $\theta_{NS}/\theta_{EW} = 1.11 \pm 0.23$. We have one observation at K, from which we obtain a 3 σ upper limit $\theta \leq 0''.045$. This star was observed at 4.6 μm and P.A. = 90° by Mariotti *et al.* (1983), who report $\theta = 0''.083 \pm 0''.051$, consistent with our measurement. Low (1979) reported an upper limit $\theta \leq 0''.083$ at 5.0 μm but a minimum size $\theta \geq 0''.25$ at 10.2 μm. Considering our upper limit at K, our measured size at M, and Low's lower limit at 10.2 μm, we conclude that the apparent angular size of the circumstellar envelope around χ Cyg also increases with wavelength.

x) *NML Cygni*

We have plotted our three-color data in Figure 10; once more it is obvious that there is a strong increase of the appar-

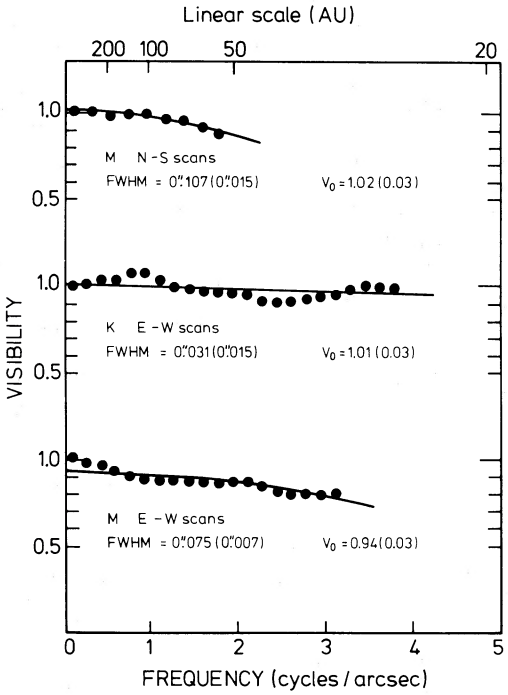

FIG. 9.—The same as in Fig. 1 except for χ Cyg

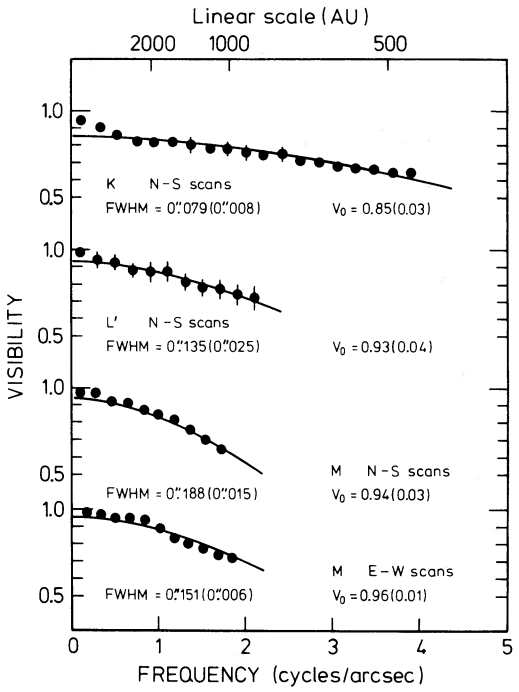

FIG. 10.—The same as in Fig. 1 except for NML Cyg

ent angular size with wavelength. Observations for this star have been reported by Low (1979) and by Sibille, Chelli, and Léna (1979) between 2.2 μm and 12.5 μm. These latter authors reported fits of uniformly bright circular disks over limited spatial-frequency intervals. Thus, their derived diameters are difficult to compare directly with our data. However, our raw visibility data appear similar to theirs. We have subjected the data in their Figures 8*a*–8*c* (taken at position angle 120°) to the same analysis as ours, which yields $\theta = 0''.053$ at 2.2 μm, $\theta = 0''.092$ at 3.3 μm, and $\theta = 0''.12$ at 4.7 μm. These values are systematically smaller than our values at corresponding wavelengths.

McCarthy (1979) reported an asymmetry at 5 μm ($\sim 0''.12 \times 0''.18$ FWHM with the long axis at P.A. $\approx 140°$–$150°$). His north-south and east-west diameters are in good agreement with our values.

A final point is that our observations at K on two different observing occasions show evidence of a halo at low spatial frequencies. The halo contributes $\sim 15\%$ of the flux at 2.2 μm and has a size $\theta = 2''$. This halo also appears in the data published by Sibille, Chelli, and Léna (1979). It was discussed by them but ultimately ruled out as a seeing artifact. We believe that the halo is real and represents a small scattering region surrounding the compact thermal dust core of the circumstellar envelope.

b) The Bipolar Nebulae

i) *AFGL 618*

We have one set of data at L' taken in the north-south direction, which we have not shown plotted in a figure. A simple Gaussian model fits the data reasonably, although, because of the source's faintness, the signal-to-noise ratio is low. Our model fit yields $\theta = 0''.13 \pm 0''.04$ and $V_0 = 0.96 \pm 0.04$. Westbrook *et al.* (1975), in their initial discussion of this source, give an angular size $\theta = 0''.4 \pm 0''.2$ at 11.2 μm. Thus, there is a large increase in size with wavelength for this source, in common with the evolved giants and supergiants just discussed.

ii) *AFGL 915*

We have obtained four-color north-south visibilities, which are plotted in Figure 11. It is clear from inspection that a simple single-component Gaussian model will not fit the data. Two components are evident in each set of data: An extended component having roughly the same size at each wavelength and a compact one whose size increases with wavelength. We identify the compact component with the thermally emitting part of the circumstellar envelope and the extended halo as a scattering region surrounding it. The models that are shown plotted in Figure 11, and for which parameters are given in Table 3, are two-component Gaussian models which quantify this description. They show that the extended region has $\theta \approx 0''.9$ at all wavelengths with a contribution to the total flux (V_0) which decreases with increasing wavelength. At H the contribution from this halo is 63%, while at M it is 33%. This decrease is less rapid than expected for purely Rayleigh-scattering particles. The compact component shows an increase in angular size and fractional flux with increasing wavelength. Low (1979) has reported a 5.0 μm size $\theta = 0''.21$ which is somewhat larger than our M size. The errors given in Table 3 for the model are determined from the range of fits permitted by the errors on individual frequency points.

iii) *OH 0739−14*

This star is included in this section because of its appearance on visual photographs (Cohen and Frogel 1977). It has also been shown to have a near-infrared spectrum characteristic of an M6 star (Allen *et al.* 1980). Our L' visibility data are shown plotted in Figure 12. Both north-south and east-west data were obtained, although at different times. The former were obtained on 1982 December 2 and the latter on 1981 November 17.

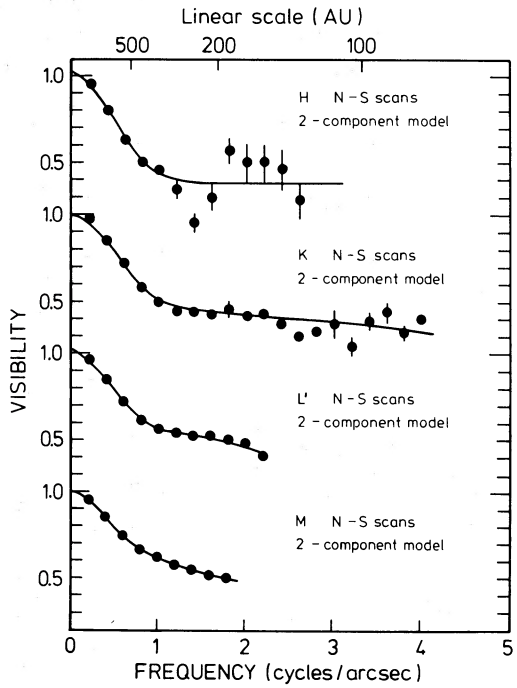

FIG. 11.—Visibility functions for AFGL 915. The solid lines represent a two-component model discussed in the text.

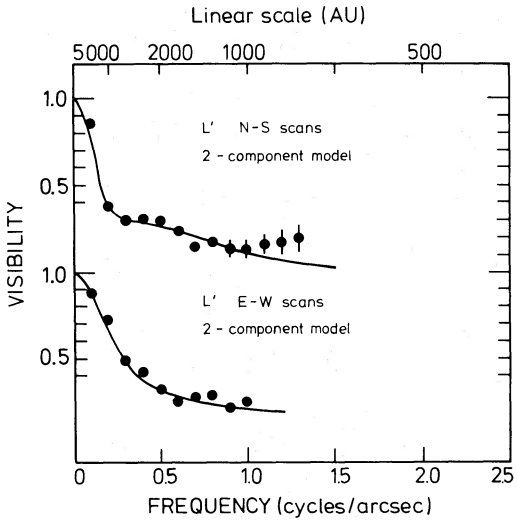

FIG. 12.—The same as in Fig. 11 except for OH 0739 − 14

As was the case for AFGL 915 the visibilities cannot be fitted by a simple Gaussian. We have fitted a two-component model to the data. The fit parameters are listed in Table 3 with the errors determined from the range of fits permitted by the errors on the individual frequency points. The models show that there is an extended region with $\theta = 3\farcs5$ north-south and $\theta = 2\farcs3$ east-west surrounding a compact core which radiates about 35% of the flux. The core itself is also resolved, with an average $\theta = 0\farcs5$, although the signal-to-noise ratio is not high. Within the errors both the extended and compact regions are symmetric. OH 0739 − 14 was also mapped previously with $1\farcs7$ and $3\farcs8$ resolution at K and L' by Allen *et al.* (1980), who did not report seeing the compact source. The extent of their L' map is $3\farcs6$ north-south by $2\farcs8$ east-west, in agreement with our measured size for the halo.

iv) *M2-9 and M1-92*

Both sources (Figs. 13–14) are resolved north-south and east-west at L'. Within the errors there is no evidence for departures from spherical symmetry.

IV. PHYSICAL DIMENSIONS OF THE CIRCUMSTELLAR ENVELOPES

The fundamental data reported here are the apparent angular sizes of circumstellar envelopes. One wishes ultimately to compute accurate physical dimensions from the apparent ones. Apart from uncertainties in the brightness distribution, which can introduce systematic errors of up to about a factor 1.6 in angular size, the greatest systematic source of error results from ignoring direct starlight. Generally, by assuming that we are not receiving any direct light from the star, as we have done in our model fits with equation (1), we derive a lower limit to the envelope diameter. In the majority of our observations the visibilities do not extend to sufficiently high spatial frequencies to allow us to estimate the stellar contribution. The fraction of direct starlight will be small when the envelope optical depth is large but can be near unity when the envelope is very optically thin. We have computed the magnitude of the effect for various hypothetical levels of direct starlight: Within the range of apparent angular diameters $0\farcs05 \leq \theta_a \leq 0\farcs2$, a 25% contribution from the star will result in a factor 1.2 underestimate in the envelope diameter. A 50% contribution results in a factor 1.6 underestimate, and 75% in a factor 2.5 underestimate. Thus, if the observed visibility at the highest spatial frequencies drops to 0.75, all we can say is that the "true" angular diameter must be in the range $\theta_a \leq \theta_{\rm true} \leq 2.5\theta_a$ and so on.

In the absence of observations which define the contribution from the underlying star, we can appeal to the models of Rowan-Robinson and Harris. We have listed corrected angular diameters in Table 4 for those stars with available models. For each wavelength we have given the contribution from the star predicted by the models and the corrected angular diameter, θ_c. Where both north-south and east-west visibilities exist in Table 3, we have listed the average value. Only χ Cyg has been omitted from the set because the models predict that more than 90% of the observed flux between 2.2 μm and 4.8 μm comes from the star. Thus, the correction factor for the observed envelope angular diameter is large and very uncertain. For IRC +10216 we have used the intermediate-scale component from our three-component visibility model, which we believe arises from thermal emission in the envelope. The models of Rowan-Robinson and Harris (1983*b*) predict a stellar contribu-

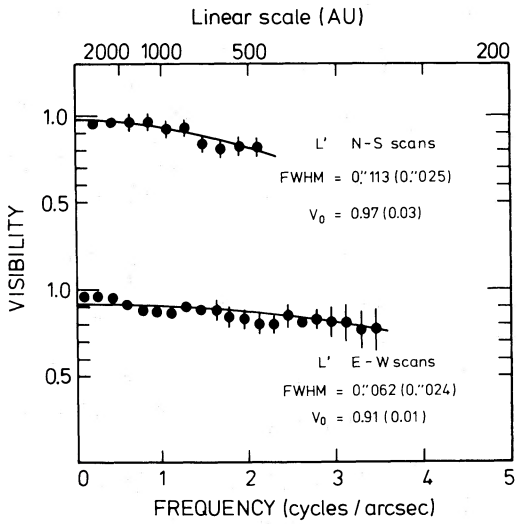

FIG. 13.—The same as in Fig. 1 except for M2-9

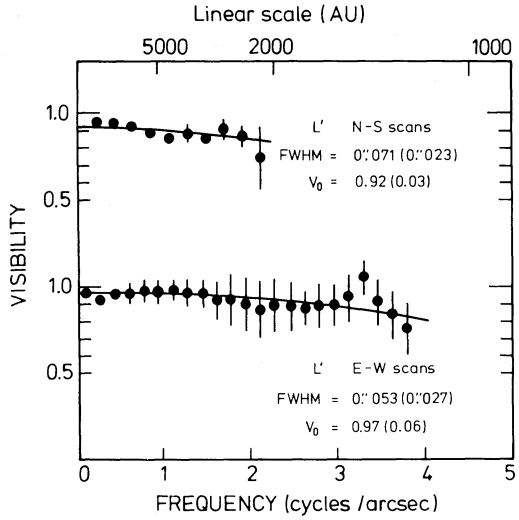

FIG. 14.—The same as in Fig. 1 except for M1-92

TABLE 4

CORRECTIONS FOR DIRECT STARLIGHT

	2.2 μm		3.8 μm		4.8 μm		
STAR	%DS[a]	θ_c (″)	%DS[a]	θ_c (″)	%DS[a]	θ_c (″)	$2\theta_1$
CIT 5	...	...	36	≤0.056	25	0.078	0.071
NML Tau	...	...	72	0.12	...	...	0.082
AFGL 915	49	0.12	14	0.14	10	0.18	0.042
VY CMa	...	...	18	0.14	14	0.16	0.116
IRC +10216	36	0.31[b]	...	...	...	...	0.356
CIT 6	74	0.16[b]	27	0.13	18	0.17	0.134
VX Sgr	45	0.070	24	0.12	...	...	0.112
OH 26.5+0.6	...	...	1	0.086[b]	1	0.133[b]	0.038
V Cyg	...	...	43	≤0.061	...	...	0.049
NML Cyg	48	0.12	19	0.16	14	0.19	0.080

[a] Percent contribution from underlying star.
[b] Average of north-south and east-west directions.

tion of 36% at 2.2 μm, and we infer 25% from our visibilities. No correction to the observed angular diameter is given because the direct contribution from the star is already taken into account in the visibility model.

The absolute size of the envelope at near-infrared wavelengths is of considerable interest. One model, which appears physically plausible, has the gas flowing out from the star driven by an (as yet) unidentified mechanism. At some critical distance, of the order of several stellar radii away from the photosphere, dust condenses, thereby forming a relatively sharp inner boundary to the dusty part of the envelope. The dust temperatures at this inner boundary are of the order of 1000 K depending upon how refractory the grains are. The region inside the inner boundary is dust free. Such a model was adopted by Sutton *et al.* (1978) to account for the observed variability of the angular diameter of Mira at 11 μm. The flux models of Jones and Merrill (1976) and Rowan-Robinson and Harris also incorporate a dust-free zone surrounded by a dusty envelope. If this concept is correct, then the measured 2–5 μm angular diameters will correspond closely to this inner boundary if the envelope is not very optically thick. Conversely, if dust exists very close to the photosphere (at significantly higher temperatures), it will radiate strongly over this wavelength range. In this case the measured near-infrared diameters will be smaller than the inner boundaries assumed in the models.

We have listed in Table 4 the predicted angular diameter of the inner boundary of the envelope, $2\theta_1$, taken from Rowan-Robinson and Harris. In the majority of cases there is good agreement between the theoretical and observed angular sizes. For all but AFGL 915 the model and observed diameters at 3.8 μm are within a factor of about 2, with the observed values being systematically larger. If the systematic difference results from an incorrect estimate of the direct contribution from starlight, it implies a smaller contribution than predicted by the models. This could, in turn, indicate the need for a slightly larger dust opacity in the near-infrared. A direct measurement of the stellar contribution is required. However, at 3.8 and 4.8 μm this is probably beyond the capability of most present ground-based telescopes. For AFGL 915 the difference between the model and the observations is a factor of 3 or more; it is unclear why the difference should be larger in this case.

In Table 5 we have given the linear radius corresponding to the distances in Table 1 for the angular diameters at 3.8 μm (except for IRC +10216, where we have used 2.2 μm). The average value of this radius is 9×10^{14} cm for eight of the ten stars in the table (i.e., excluding those with upper limits only). The stars with the largest radii are VY CMa, VX Sgr, and NML Cyg, all oxygen-rich. Three of the four stars with the smallest radii are carbon stars (CIT 5, CIT 6, and V Cyg).

The increase of angular diameter with wavelength, discussed in the previous section, is also still apparent in Table 4 even after correction for direct starlight. In Figures 15 and 16 we have plotted our corrected data for VY CMa, AFGL 915, NML Cyg, IRC +10216, and CIT 6 together with other interferometric data taken from the literature (described in § III). In

TABLE 5

COMPARISON OF INFRARED AND RADIO SIZES

Star	$\theta_{3.8}$ (″)	R_{IR} (cm)	θ_{SiO} (″)	θ_{H_2O} (″)	θ_{OH} (″)	Ref.
CIT 5	≤0.056	$\leq 3 \times 10^{14}$	...	...	...	
NML Tau	0.12	2.4×10^{14}	...	...	5.9	1
AFGL 915	0.14	3.5×10^{14}	...	...	...	
VY CMa	0.14	1.6×10^{15}	0.050:	0.20	4.2	2, 3, 4
IRC +10216	0.31	6.7×10^{14}	...	...	...	
CIT 6	0.13	1.9×10^{14}	...	...	...	
VX Sgr	0.12	1.4×10^{15}	0.070	0.25	4.6	4, 5, 6
OH 26.5+0.6	0.086	7.1×10^{14}	...	...	7.0	3
V Cyg	≤0.061	$\leq 3 \times 10^{14}$	...	...	...	
NML Cyg	0.16	2.2×10^{15}	...	...	6.0	3

REFERENCES.—(1) Baud and Habing 1983. (2) Rosen *et al.* 1978. (3) Bowers, Johnston, and Spencer 1983. (4) Lane 1982. (5) Moran *et al.* 1984 (quoted by Snyder 1980). (6) Baud 1981.

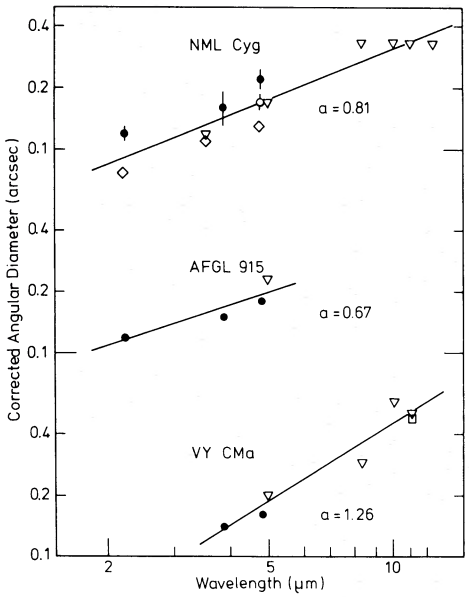

FIG. 15.—Plot of the angular diameter, corrected for direct starlight, vs. wavelength for two oxygen-rich stars and AFGL 915.

the latter case, corrections for direct starlight have been applied when $\lambda \leq 5$ μm; for longer wavelength data no corrections have been applied because the models predict a stellar contribution of less than 10%. Data taken at all position angles and epochs have been plotted. Thus, the scatter may reflect both time variations and azimuthal intensity asymmetries as well as statistical and systematic errors. Each of the five data sets has been fitted by a power law of the form $\theta \propto \lambda^{\alpha}$. The exponent $\alpha \approx 0.2$ for CIT 6 and IRC +10216, the two carbon stars shown in Figure 16. For the two oxygen-rich stars shown in Figure 15, $0.7 \leq \alpha \leq 1.3$. Thus, the carbon-star envelopes apparently show a shallower wavelength dependence of θ than do the oxygen-star envelopes. This difference between the two classes of stars probably reflects the different envelope dust opacities. The increase of angular size with wavelength is a natural consequence of models with a central heat source. For carbon stars, the models of Rowan-Robinson and Harris (1983*b*) show a larger size at 10 μm than at 2 μm. For oxygen stars they (Rowan-Robinson and Harris 1983*a*) predict a monotonic increase of size between 2 and 10 μm. Their models appear to show a slower increase with wavelength for the carbon stars, consistent with our observations.

In Table 5 we have compared our 3.8 μm angular sizes with those for various molecules in the radio spectral region. The OH masers are found in a part of the shell whose angular diameter is a factor of about 50 greater than the part radiating most of the 3.8 μm flux. The SiO and H_2O masers, by comparison, are located near the infrared diameter. From the limited data available, the hierarchy appears to be $\theta_{SiO} < \theta_{3.8\,\mu m} < \theta_{H_2O}$. If $\theta_{3.8\,\mu m}$ is interpreted as the dust formation boundary, then that boundary would lie between the two masing regions. This suggests two speculations: (1) SiO masers may not exist beyond $\theta_{3.8\,\mu m}$ because the molecules are locked up in grains forming at this inner boundary. (2) The range of radial velocities for the H_2O masers may be expected to be larger than for the SiO masers because the H_2O molecules are dragged along to higher expansion velocities by the newly formed grains, which experience significant radiation pressure from the star.

V. ANGULAR DIAMETERS AND MASS LOSS RATES

Gehrz and Woolf (1971) first showed that one could infer stellar mass loss rates from infrared observations, if the flows of the grains and gas are coupled. If the envelopes are all very optically thin, one should see no dependence of angular size upon mass loss rate. For this case one observes the radius in the envelope where grains condense, which depends mainly upon the properties of the stellar radiation field. Under other conditions, however, one may expect to observe a relationship between the envelope size and the mass loss rate. If the envelopes were all optically thick and isothermal, for example, one would measure the radius at which the optical depth is approximately unity. For this case the mass loss rate is

$$\dot{M} = \frac{4\pi}{k} VR ,$$

where R is the radius in the envelope at which the optical depth is unity, V is the mass flow velocity at R, and k is the total mass absorption coefficient. If the velocity at R is related to the terminal velocity, V_0, through a (nearly) constant factor, then we have the (approximate) proportionality

$$\frac{\dot{M}}{V_0} \propto D\theta ,$$

where D is the distance to the object, and θ is the observed angular diameter.

Real envelopes will, of course, be neither completely optically thin nor isothermal. The relationship between mass loss rate and angular diameter will be a complex function of the temperature and density. In this case it is not so simple to predict in advance how it would appear, although something between the two extremes discussed above may be reasonably expected. In Figure 17 we have plotted $\log(\dot{M}/V_0)$ (from Table 1) versus $\log(D\theta)$. We have used the measured angular diameter at 3.8 μm, whenever possible, but have made no corrections for direct starlight in order to obtain the largest possible sample of stars. One sees that an approximately linear relationship exists over three decades of $\dot{M}/V_0$. Fitting a power law to the data yields a proportionality of the form

$$\frac{\dot{M}}{V_0} \propto (D\theta)^{1.3} .$$

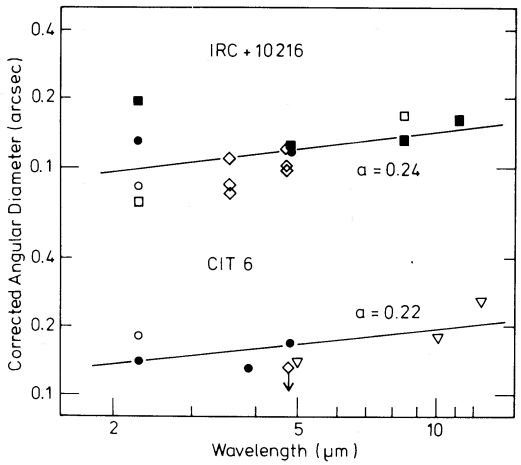

FIG. 16.—Plot of the angular diameter, corrected for direct starlight, vs. wavelength for two carbon stars.

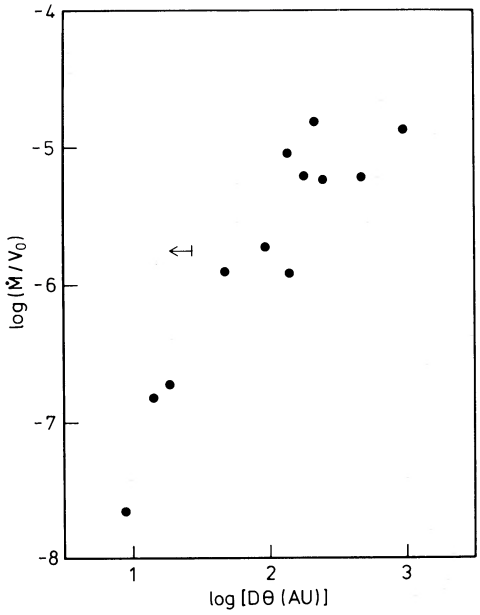

FIG. 17.—Plot of log $(\dot{M}/V_0)$ vs. log $(D\theta)$. No corrections for direct starlight have been applied.

This is close to that predicted from the simple assumptions that the shell is isothermal and optically thick. However, the relation will be steeper when proper corrections for direct starlight are included. This is because the direct contribution will affect the optically thinner envelopes, which tend to be those with the lowest $\dot{M}/V_0$, more than the thicker ones.

Although we do not want to discuss here the reasons for the form of the observed relation, the important point remains that a relationship does exist in the expected sense: Objects with higher mass loss rates have significantly larger angular diameters than those with smaller rates.

VI. SUMMARY

We have presented near-infrared visibility functions for 16 late-type giants and supergiants and bipolar nebulae. The principal results of the study are as follows.

1. Many infrared-bright stars with dense circumstellar dust envelopes are at least partially resolvable from the ground by speckle interferometry.

2. If the near-infrared diameters are interpreted as the inner boundary for dust in the envelope, this boundary has a radius of order 10^{15} cm, plus or minus a factor of 3.

3. The observed angular diameters agree to within a factor of about 2 with model diameters, with or without correction for light from the underlying star.

4. The envelope diameters show a systematic increase with wavelength. Carbon stars appear to have a shallower increase than oxygen stars. Both of these observations are in agreement with models in the literature.

5. There is a systematic increase of the apparent angular diameter of the dust envelope with increasing mass loss rate.

6. At our present spatial resolution, it is difficult to measure spatial asymmetries for all but the most extended objects.

7. A number of the objects show clear indication of the existence of two spatial components having different scale sizes. The larger of the components is interpreted as a scattering region surrounding the smaller, thermal emission region.

Future progress can be made in several important areas: (i) complete resolution of the envelope with a clear separation of the underlying star; (ii) full or partial image reconstruction of the envelope to reveal any asymmetries in the mass loss process; and (iii) much wider wavelength coverage. Of these, (i) may be of most immediate importance for constraining existing models.

We would like to thank U. Carsenty, S. Harris, M. Jura, Th. Reddmann, L. Snyder, R., Wolstencroft, and E. Wright for useful discussions and correspondence during the course of this work. B. Z. acknowledges partial support from NSF grant AST 80-23355 to the University of Maryland. H. M. D. acknowledges partial support from NSF grant AST 82-08793 to the University of Hawaii.

REFERENCES

Allen, D. A., Barton, J. R., Gillingham, P. R., and Phillips, B. A. 1980, *M.N.R.A.S.*, **190**, 531.
Allen, D. A., Barton, J. R., and Wallace, P. T. 1981, *M.N.R.A.S.*, **196**, 797.
Baud, B. 1981, *Ap. J.* (Letters), **250**, L79.
Baud, B., and Habing, H. J. 1983, *Astr. Ap.*, **127**, 73.
Bowers, P. F., Johnston, K. J., and Spencer, J. H. 1983, *Ap. J.*, **274**, 733.
Carsenty, U. 1983, Ph.D. thesis, Ruprecht-Karls-Universität, Heidelberg.
Cohen, J. G., and Frogel, J. A. 1977, *Ap. J.*, **211**, 178.
Cohen, M., *et al.* 1975, *Ap. J.*, **213**, 66.
Deutsch, A. J. 1960, in *Stars and Stellar Systems*, Vol. **6**, *Stellar Atmospheres*, ed. J. L. Greenstein (Chicago: University of Chicago Press), chap. 15.
Dyck, H. M., and Howell, R. R. 1982, *A.J.*, **87**, 400.
Eiroa, C., Hefele, H., and Qian Zhong-yu. 1983, *Astr. Ap. Suppl.*, **54**, 309.
Gehrz, R. D., and Woolf, N. J. 1971, *Ap. J.*, **165**, 285.
Gillett, F. C., Merrill, K. M., and Stein, W. A. 1971, *Ap. J.*, **164**, 83.
Herbig, G. H. 1972, *Ap. J.*, **172**, 375.
———. 1975, *Ap. J.*, **200**, 1.
Howell, R. R. 1980, Ph.D. thesis, University of Arizona.
Hyland, A. R., Becklin, E. E., Frogel, J. A., and Neugebauer, G. 1972, *Astr. Ap.*, **16**, 204.
Jones, T. W., and Merrill, K. M. 1976, *Ap. J.*, **209**, 509.
Knapp, G. R., Phillips, T. G., Leighton, R. B., Lo, K. Y., Wannier, P. G., and Wootten, H. A. 1982, *Ap. J.*, **252**, 616.
Kwan, J., and Linke, R. A. 1982, *Ap. J.*, **254**, 587.
Lane, A. P. 1982, Ph.D. thesis, University of Massachusetts.
Lefèvre, J., Bergeat, J., and Daniel, J.-Y. 1982, *Astr. Ap.*, **114**, 341.
Lefèvre, J., Daniel, J.-Y., and Bergeat, J. 1983, *Astr. Ap.*, **121**, 51.
Leinert, Ch., and Dyck, H. M. 1983, *Appl. Optics*, **22**, 2403.
Low, F. J. 1979, in *IAU Colloquium 50, High Angular Resolution Stellar Interferometry*, ed. J. Davis and W. J. Tango (Sydney: Chatterton Astronomy Department, University of Sydney), p. 2-1.
Mariotti, J. M., Chelli, A., Foy, R., Léna, P., Sibille, F., and Tchountonov, G. 1983, *Astr. Ap.*, **120**, 237.
McCammon, D., Münch, G., and Neugebauer, G. 1967, *Ap. J.*, **147**, 575.
McCarthy, D. W. 1979, in *IAU Colloquium 50, High Angular Resolution Stellar Interferometry*, ed. J. Davis and W. J. Tango (Sydney: Chatterton Astronomy Department, University of Sydney), p. 18-1.
McCarthy, D. W., Howell, R. R., and Low, F. J. 1980, *Ap. J.* (*Letters*), **235**, L27.
Merrill, K. M., and Stein, W. A. 1976, *Pub. A.S.P.*, **88**, 294.
Moran, J. M., *et al.* 1984, in preparation.
Neugebauer, G., and Leighton, R. B. 1969, *Two-Micron Sky Survey, A Preliminary Catalogue* (NASA SP-3047).
Neugebauer, G., Martz, D. E., and Leighton, R. B. 1965, *Ap. J.*, **142**, 399.
Perrier, C. 1982, Thèse de Doctorat de 3ème cycle, Université de Paris.
Reid, M. J., Moran, J. M., and Johnston, K. J. 1981, *A.J.*, **86**, 897.
Rosen, B. R., Moran, J. M., Reid, M. J., Walker, R. C., Burke, B. F., Johnston, K. J., and Spencer, J. H. 1978, *Ap. J.*, **222**, 132.
Rowan-Robinson, M., and Harris, S. 1982, *M.N.R.A.S.*, **200**, 197.
———. 1983*a*, *M.N.R.A.S.*, **202**, 767.
———. 1983*b*, *M.N.R.A.S.*, **202**, 797.
Selby, M. J., Wade, R., and Sanchez Magro, C. 1979, *M.N.R.A.S.*, **187**, 553.
Sibille, F., Chelli, A., and Léna, P. 1979, *Astr. Ap.*, **79**, 315.
Snyder, L. E. 1980, in *IAU Symposium 87, Interstellar Molecules*, ed. B. H. Andrew (Dordrecht: Reidel), p. 525.

Spergel, D. N., Giuliani, J. L., and Knapp, G. R. 1983, *Ap. J.*, **275**, 330.
Sutton, E. C., Betz, A. L., Storey, J. W. V., and Spears, D. L. 1979, *Ap. J. (Letters)*, **230**, L105.
Sutton, E. C., Storey, J. W. V., Betz, A. L., Townes, C. H., and Spears, D. L. 1977, *Ap. J. (Letters)*, **217**, L97.
Sutton, E. C., Storey, J. W. V., Townes, C. H., and Spears, D. L. 1978, *Ap. J. (Letters)*, **224**, L123.
Tielens, A. G. G. M. 1983, *Ap. J.*, **271**, 702.
Toombs, R. I., Becklin, E. E., Frogel, J. A., Law, S. K., Porter, F. C., and Westphal, J. A. 1972, *Ap. J. (Letters)*, **173**, L71.
Tsuji, T. 1979, *Pub. Astr. Soc. Japan*, **31**, 43.
Westbrook, W. E., Becklin, E. E., Merrill, K. M., Neugebauer, G., Schmidt, M., Willner, S. P., and Wynn-Williams, C. G. 1975, *Ap. J.*, **202**, 407.

S. Beckwith: Department of Astronomy, Cornell University, Ithaca, NY 14853

H. M. Dyck: Institute for Astronomy, 2680 Woodlawn Drive, Honolulu, HI 96822

Ch. Leinert: Max-Planck-Institut für Astronomie, Königstuhl, D-6900 Heidelberg 1, Federal Republic of Germany

B. Zuckerman: Department of Astronomy, University of California, Los Angeles, CA 90024